Virtual operational strength analysis for commercial vehicles

Robert Buchmann[1,2], Dr. Roland Krivachy[2], Prof. Dr. Alexander Lion[1]

[1] Bundeswehr University, Germany
[2] MAN Truck & Bus SE, Germany

Abstract. Customer demands and governmental emission regulations require new lightweight and electro mobility concepts in the commercial vehicle market. The necessary design changes have a significant impact on both, the structural strength and the dynamics of the chassis and the body. The evaluation of the chassis components and the body in terms of structural dynamics and operational strength at an early stage of the development process plays an important role for a time and cost effective validation process. Using simulation methods, the virtual vehicle can be analyzed long before a physical prototype is available which allows faster structural design optimizations. The virtual rough road testing combines multiple simulation disciplines and takes the full vehicle dynamics into account. Starting with the full finite element model for strength analysis, a superelement is generated using component mode synthesis. This superelement is incorporated in multibody rough road simulation to consider the elastic body deformations. The multiaxial loading history and the material data of all components are subsequently used in the operational strength analysis to determine the resulting hotspot regions and to derive structural optimizations. For a reliable operational strength forecast, an accurate prediction of the input load history is important. Therefore, the modelling of the front axle used in city busses is investigated. A flexible model of the axle is used for a stress comparison with real world test track data. In a further step, the necessity of the flexible body is evaluated with a comparison of the resulting bushing forces attached to the frame structure.

Keywords: Operational Strength, Flexible Bodies, Load Validation.

1 Introduction

One of the core keys of Europe´s economy is the efficient transport of goods and people. In the transportation sector, the customer demands in terms of cost effectiveness, comfort and driver-assistance systems as well as governmental emission regulations are rising. Together with a high number of variants along with comparable small production numbers the complexity of the development process for new vehicle generations increases. In order to fulfill the demands for future vehicles, new lightweight structures

P. E. Pfeffer (ed.), *11th International Munich Chassis Symposium 2020*,
Proceedings, https://doi.org/10.1007/978-3-662-63193-5_22

and powertrain concepts are developed. The design changes have a significant impact on both the structural strength and the dynamics of the chassis and the body. The evaluation of the chassis components and the body in terms of structural dynamics and operational strength at an early stage of the development process plays an important role for a time and cost effective validation process. Currently, rough road testing for reference vehicles and comparative simulations for variants are used for the final operational strength approval. Using simulation methods, the virtual vehicle can be analyzed long before a physical prototype is available which allows faster structural design optimizations. Virtual fatigue simulations hence offer the possibility of carrying out strength evaluations at an early stage of the development process, as physical rough road tests can only be carried out at a late stage when prototype vehicles are available.

2 Durability testing of vehicles

Repetitive loading of a metallic structure leads to fatigue of the material. The amount of cycles the material can withstand depends on the load characteristic, the geometry and the material properties. In order to prevent structural failures of vehicles in the field durability tests are performed that incorporate the customer service loads. In this chapter a brief overview over physical and virtual methods for determining the fatigue life of the entire vehicle structure is presented.

2.1 Physical durability testing

In order to accomplish the required number of loading events specified for a new vehicle in the mission profile, different approaches exist. The physical testing of structures is extremely time consuming because the accumulation of fatigue damage depends on the number of load cycles. Therefore, principles for accelerated testing are commonly used in order to avoid the accurate, but time consuming, long term testing under customer service conditions. Halfpenny [2] classified the methods in three categories.

- Compressed time
- Load amplification
- Combined

The rough road and test rig testing described in the following are a combined accelerated approach. They make use of amplified loads and disregard non-damaging load sequences.

Rough road testing. The rough road testing at MAN consists of multiple test tracks that are repeated several times in a strict order. The test tracks include various road conditions and obstacles, with exaggerated dimensions for a reduced number of cycles necessary. Non-damaging parts of real world customer service loads are omitted by the construction of the test tracks. The different test tracks at MAN Truck and Bus for durability testing are shown in figure 1.

Fig. 1. MAN test track seen from above [3]. Different road conditions and obstacles are used for the rough road testing.

Road simulation test rig. A further reduction in required time can be achieved with road simulation test rigs. The vehicle is therefore placed on a system of cylinders that reproduce the operational loads from the rough road test tracks. The operational loads are either measured signals from rough road testing or taken from simulation models. The test rig requires a minimal human involvement and makes a continuous testing possible. The advantages compared to rough road testing are reduced time and costs, with the challenging task of choosing the appropriate input signal. A full physical and virtual vehicle test rig used for busses and trucks is displayed in figure 2.

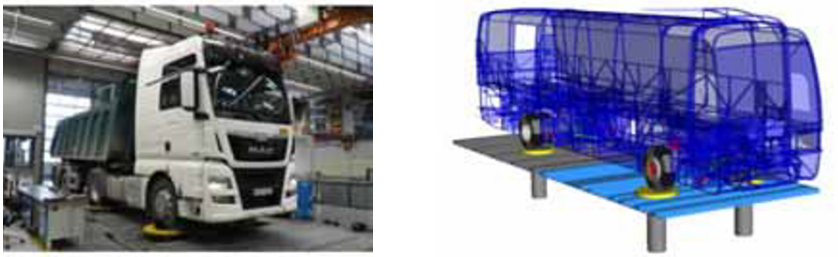

Fig. 2. Physical (left) and virtual (right) hydraulic test rig for trucks and busses. The virtual test rig uses a multibody simulation model with a flexible frame structure

2.2 Virtual durability testing

Virtual durability testing methods do not require physical prototypes and can thus be performed in earlier stages in development processes [1,4]. They rely on simulations models to analyze the lifetime of the structure and consist of three subsequent steps. In a first step, an appropriate load history needs to be generated. This can be done either from experience, experiments or simulation. In a second step, a stress analysis using a finite element model of the structure with the defined load history is performed. The evaluation of the fatigue strength can either directly rely on the stress distribution or on

a subsequent fatigue life assessment taking both the load cycle information and the material fatigue properties into account.

Static and quasi-static load cases. Equivalent static load cases derived from real world measurements or dynamic simulations, combined with a vast experience, are a fast method to predict the fatigue of the vehicle structure. The load cases contain different scenarios during customer service such as braking, accelerating and cornering that are separately applied to the finite element model of the structure. Based on the calculated stresses, the durability is evaluated. The transformation of the load histories into equivalent static load cases is a challenging task, lacks accuracy and is not always possible as vibration phenomena and dynamic effects are not captured [4,5].

The static load cases can be extended to harmonic frequency excitations under consideration of the inertia relief method. This permits an insight into the basic dynamical behavior. The dynamic behavior under constant harmonic frequency excitation is studied to compute the stress distribution due to sinusoidal input loads. Both static and quasi-static load cases provide fast and, together with a vast experience, reliable results for classic vehicle concepts. New disruptive vehicle structures due to lightweight and electro mobility demands can only be assessed to a limited detail level since vibration phenomena are not captured and the load prediction is not accurate [4].

Virtual rough road simulation. For a detailed fatigue life evaluation considering dynamic effects and vibration phenomena of the vehicle structure, rough road testing is performed virtually. The virtual rough road testing is a multidisciplinary fatigue life assessment approach, incorporating finite element- and multibody-simulations, with a subsequent stress cycle-based fatigue life estimation. In this process, the digital twin of the test track of the real world rough road are used for an accurate load history prediction. The single steps of the process are illustrated in figure 3.

The finite element model used for the strength analysis of the vehicle structure is too large for a transient simulation in the time domain. Therefore, a superelement of it is derived using the technique of component mode synthesis. The reduced order model consists of Eigenmodes and additional static attachment modes. The use of additional attachment modes improves the static response of the structure to loads acting at the connection points of the structure to other components, such as the axles, the engine and the steering [6].

The superelement is then integrated in the multibody simulation model of the vehicle and connected to the drivetrain and axle models. In the multibody simulation domain, the superelement of the structure is called a flexible body. It permits elastic deformations of the structure and takes dynamic effects into account, such as vibration phenomena. This allows an accurate prediction of the time-dependent loads and stresses when driving over the digital test tracks. The stresses are calculated based on the modal participation factors from the multibody simulation and the unit load stresses obtained for each normal and attachment mode from the finite element analysis.

The calculated stress history is post processed with the Rainflow counting method to obtain a set of stress reversals. This set can be efficiently handled using the Miner´s rule to calculate the local fatigue life prediction. The local fatigue life values are then evaluated to optimize the structure. This can either be reinforcements to strengthen the structure in critical areas or lightweight modifications in uncritical areas.

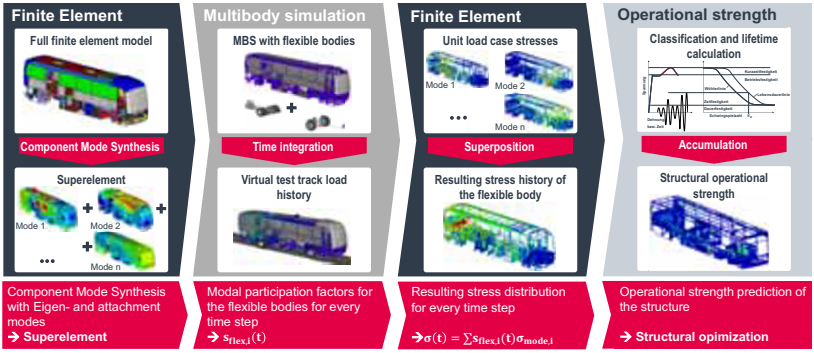

Fig. 3. Simulation process for virtual rough road testing

3 Flexible Bodies in multi body simulation

The classical multibody simulation approach assumes rigid bodies, meaning the deformability of the body is ignored. If the deformations of the body to be modelled are negligible or unimportant, this assumption provides a simple modelling and short computation times. If the deformations of the body become important, the elastic behavior has to be taken into account.

3.1 Flexible body representation

In this subsection, the general approach for a flexible representation of bodies in multibody simulation is shown. Further explanations can be found in [7,8,9]. The position of a volume element dV of a body can be described by a position vector for the undeformed state $\mathbf{u_r}$ and the elastic displacement $\mathbf{u_e}$. Both vectors depend on the location $\mathbf{c}$ of the volume element and time t.

$$\mathbf{u}(\mathbf{c}, t) = \mathbf{u_r}(\mathbf{c}, t) + \mathbf{u_e}(\mathbf{c}, t) \tag{1}$$

Assuming small deformations, the elastic deformation can be approximated by a modal representation following the Ritz approach, where the displacements are expressed by a linear combination of mode shapes $\mathbf{u_j}(\mathbf{c})$ and time dependent scalar weighting functions $q_j(t)$.

$$\mathbf{u_e}(\mathbf{c}, t) \approx \sum_{j=1}^{m} \mathbf{u_j}(\mathbf{c}) q_j(t) \tag{2}$$

The position of a volume element dV consequently depends on the rigid bod coordinates $\mathbf{u_r}$ and a displacement $\mathbf{u_e}$ that is approximated by m Eigenmodes and particular modes. The quality of the approximation depends on the number of mode shapes and their appropriateness to capture the dynamic boundary value problem. The vehicle structure in the multibody simulation model is subjected to inertia forces and reaction forces acting in the constraints and force elements attached to it. It is therefore necessary for the modal stress calculation to consider, in addition to Eigenmodes, particular mode shapes such as static or inertia relief modes. The approach to derive both the Eigenmodes of the free structure and the inertia relief attachment modes is outlined in the following section.

3.2 Component Mode Synthesis

Component mode synthesis reduces the system matrices of the full finite element model to a smaller set of interface degrees of freedom and a truncated set of generalized coordinates. A detailed derivation of the presented approach is found in [6,10]. For a damped system, the governing equation of the full model can be written in the following form with mass matrix **M**, stiffness matrix **K** and damping matrix **C**. The vector **f** contains the external forces acting on the structure.

$$\mathbf{M\ddot{u}} + \mathbf{C\dot{u}} + \mathbf{Ku} = \mathbf{f} \tag{3}$$

The physical displacement coordinates **u** are approximated in terms of generalized coordinates **q** using the Ritz approach in component mode synthesis.

$$\mathbf{u} = \mathbf{Tq} \tag{4}$$

Equation (3) can then be written as

$$\mathbf{MT\ddot{q}} + \mathbf{CT\dot{q}} + \mathbf{KTq} = \mathbf{f} + \mathbf{r}. \tag{5}$$

The residual force **r** results from the approximation made with the transformation if only a truncated set of generalized coordinates is used and can be eliminated with the Galerkin projection.

$$\mathbf{T^T r} = \mathbf{0} \tag{6}$$

Equation (3) then becomes

$$\mathbf{\hat{M}\ddot{q}} + \mathbf{\hat{C}\dot{q}} + \mathbf{\hat{K}q} = \mathbf{\hat{f}} \tag{7}$$

with the reduced mass matrix $\mathbf{\hat{M}} = \mathbf{T^T MT}$, the reduced damping matrix $\mathbf{\hat{C}} = \mathbf{T^T CT}$, the reduced stiffness matrix $\mathbf{\hat{K}} = \mathbf{T^T KT}$ and the transformed load vector $\mathbf{\hat{f}} = \mathbf{T^T f}$.

Component modes. The component mode synthesis consists of different sets of modes: normal modes, attachment or constraint modes and rigid body modes. A constraint

mode is the static deformation of the structure due to a unit displacement of one interface node while restraining the other interface nodes and keeping all other nodes force-free. Attachment modes are defined as the displacement vector due to a unit force applied to a single interface node. A rigid body mode describes the undeformed configuration of the structure due to a unit displacement with all forces on the component set to zero and can be seen as a special case of a constraint mode. The normal modes are the Eigenmodes of the structure and are classified according to the interface boundary condition. For the fixed method these are the fixed-interface normal modes and for the free method these are the free-interface normal modes. The free-interface normal mode $\boldsymbol{\phi}_j$ is calculated from

$$\left(\mathbf{K} - \omega_j^2 \mathbf{M}\right)\boldsymbol{\phi}_j = \mathbf{0}\ j = 1,2, \ldots N_f \tag{8}$$

with the corresponding Eigenfrequency ω_j up to a specified number N_f of modes or a frequency limit. Only a small subset of normal modes is used to approximate the dynamic behavior in model order reduction schemes. This approach is called mode truncation, assuming that the description of the dynamic properties of the component is still sufficient with the small subset.

Free-interface method. In this work, the free-interface method is used with inertia relief attachment modes. The derivation of the transformation matrix is presented in the following.

The nodal displacement vector u can be partitioned in a set of master degrees of freedom $\mathbf{u_m}$ and internal slave degrees of freedom $\mathbf{u_s}$**.** External forces are only applied to the master degrees of freedom.

$$\mathbf{u} = \begin{bmatrix} \mathbf{u_m} \\ \mathbf{u_s} \end{bmatrix} \tag{9}$$

Neglecting the damping forces equation (3) can be written as

$$\begin{bmatrix} \mathbf{M_{mm}} & \mathbf{M_{ms}} \\ \mathbf{M_{sm}} & \mathbf{M_{ss}} \end{bmatrix} \begin{bmatrix} \ddot{\mathbf{u}}_\mathbf{m} \\ \ddot{\mathbf{u}}_\mathbf{s} \end{bmatrix} (t) + \begin{bmatrix} \mathbf{K_{mm}} & \mathbf{K_{ms}} \\ \mathbf{K_{sm}} & \mathbf{K_{ss}} \end{bmatrix} \begin{bmatrix} \mathbf{u_m} \\ \mathbf{u_s} \end{bmatrix} (t) = \begin{bmatrix} \mathbf{f_m} \\ \mathbf{f_s} \end{bmatrix} (t). \tag{10}$$

In the free-interface method in ANSYS [11], the generalized coordinates contains three sets of modes: constraint modes $\mathbf{p_r}$, inertia relief attachment modes $\mathbf{p_d}$ and free-interface normal modes $\mathbf{p_k}$**.** Thus, the transformation matrix for the free-interface method takes the form

$$\mathbf{u} = \begin{bmatrix} \mathbf{u_m} \\ \mathbf{u_s} \end{bmatrix} = \begin{bmatrix} \mathbf{I} & \mathbf{0} & \mathbf{0} \\ \mathbf{G_{sm}} & \boldsymbol{\Phi}_\mathbf{sr} & \hat{\boldsymbol{\Phi}}_\mathbf{s} \end{bmatrix} \begin{bmatrix} \mathbf{p_r} \\ \mathbf{p_d} \\ \mathbf{p_k} \end{bmatrix} \tag{11}$$

As pointed out in [6], rigid body modes are a special case of constraint modes. So, the first column of the transformation matrix **T** contains the constraint mode data. In the second column, the inertia relief mode data is stored and the third column contains the normal mode data. The components of the transformation matrix are briefly described,

a more detailed explanation can be found in [6] and [11]. The matrix $\mathbf{\Phi_{sr}}$ contains the inertia relief attachment modes. The matrix $\widehat{\mathbf{\Phi}}_\mathbf{s}$ is calculated from the slave partition, meaning the interior nodes of the free-interface normal modes $\mathbf{\Phi_s}$, the master partition (interface nodes) of the free-interface normal modes $\mathbf{\Phi_m}$ and the constraint mode matrix $\mathbf{G_{sm}}$.

$$\widehat{\mathbf{\Phi}}_\mathbf{s} = \mathbf{\Phi_s} - \mathbf{G_{sm}}\mathbf{\Phi_m} \tag{12}$$

The inclusion of the inertia relief attachment modes is important for the accuracy of the reduced order model if the free method is applied and only a truncated set of free-interface modes is used [6,10].

4 Flexible model of the front axle

One important aspect for a reliable simulation of the fatigue life is a good estimate of the input load history. While for the multibody simulation model of the rear axle of the bus a validation of the input loads was already conducted, the input loads from the front axle were so far not yet validated in detail. The measurement of the bushing forces during the rough road sections is a challenging task, as their mechanical behavior is highly nonlinear. For the assessment of the front axle components measurements with strain gauges were conducted to approve the axle components fatigue strength. These measurements are used in the following for a validation of the front axle input loads. A flexible model of the front axle allows a direct evaluation of the component stress history on a test track simulation. Assuming that the stress distribution in the hardware and modelled component matches, the resulting forces acting on the structure are comparable.

4.1 Front axle modelling

For an improved ride comfort and good maneuverability, a double wishbone axle is used for the new city bus generation Lion´s City at MAN. The lower arm is a single wishbone whereas the upper arm consists of two single arms connected with a bolt. The lower and upper wishbones are connected with bearings to a knuckle. The wheel carrier is connected to the knuckle to allow the steering. The front axle is displayed in figure 4 and was so far modelled with rigid bodies in the MBS connected with bushings to the frame structure. For the validation of the stresses in the axle components, a flexible modelling of the wishbones, the connecting bolts and the knuckle is introduced. In figure 4, the lower wishbone is shown in blue, the upper wishbone in yellow and the knuckle in red. The axle components were modelled with second order tetra elements and an average mesh size of 8 mm.

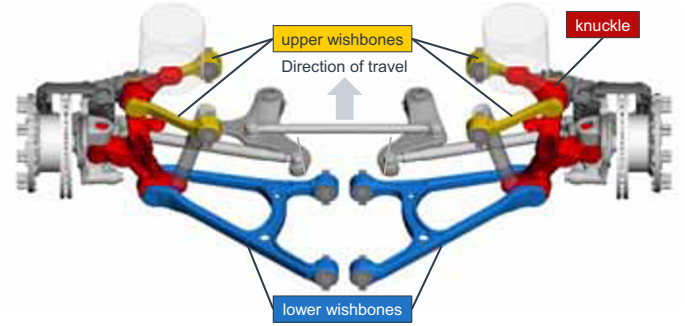

Fig. 4. Multibody Simulation Model of the front axle with wishbones and knuckles

4.2 Model variants

Besides the flexible modelling of the frame, the flexible modelling of the front axle leads to longer simulation times and increases the complexity of the model. For a full validation of the axle, the wishbones and knuckles are modelled as flexible bodies to compare the stress results with the measurements. The effect of the flexibility of the components on the resulting input loads is investigated with different variants shown in table 1. Starting with the rigid variant the lower arm is modelled as a flexible body in variant 1. Variant 2 also includes deformable upper wishbones and variant 4 is extended to a flexible knuckle.

Table 1. Investigated variants of the front axle

Variant	lower wishbone	upper wishbone	knuckle
1	rigid	rigid	rigid
2	flexible	rigid	rigid
3	flexible	flexible	rigid
4	flexible	flexible	flexible

4.3 Application of virtual stain gauges

For a validation with measured strains via strain gauges during the rough road testing, a similar approach is needed in the virtual world. Therefore, the flexible bodies were equipped with virtual strain gauges at the measurement locations in the MBS software SIMPACK. In a first step, the location of the strain gauges on the physical components were taken from a measurement map and pictures. Based on that, the location an orientation of the strain gauges is determined and the node closest to the corresponding position is selected to a set in the finite element model. The nodes contained in the set can later be used as masternodes during the model order reduction process. The selection as masternodes during the reduction process allows the creation of a deformed marker in the MBS at this position. A deformed marker moves with the respective body such

that its position and orientation are dependent on the body deformation. For small elastic deformations of the body, also the use of an undeformed marker with the correct orientation is sufficient as a reference marker. This undeformed marker captures the rigid body motion, but the elastic deformation is ignored. The general process is illustrated in figure 5. In the physical testing, the strain gauges are applied to the components and then the whole front axle is assembled. Before the measurement is started, the vehicle is placed on an even surface and all mounted strain gauge signals are set to zero, such that the static stresses are ignored. In the multibody simulation, the virtual strain gauges are applied to the components to measure the static and dynamic parts. In order to remove the static part and for a comparison with the test data, an additional static maneuver is added. The static stresses are then subtracted from the test track maneuver simulations.

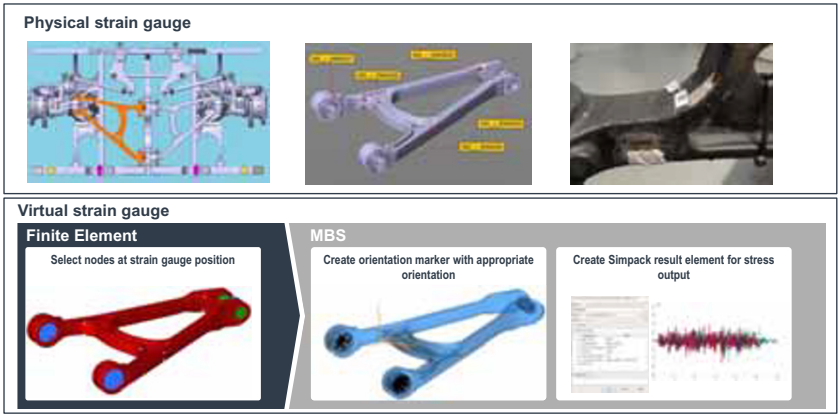

Fig. 5. Process for the application of virtual strain gauges in the multibody simulation for a comparison with real world strain gauge results

5 Results

In this section, a comparison of the simulated stresses with measured ones is presented. For a better interpretation of the measurement results, the measured strains are converted to stresses using the Young´s moduli of the components. Therefore, the comparison will be made using stress values. Furthermore, the necessity to model the axle with flexible bodies is investigated, comparing the bushing forces at the frame.

5.1 Comparison of simulated stress with measurements

In this subsection, the stress results for different test track sections and strain gauges are presented. Analyzing the location and measured strain histories, not all of the available strain gauges from the measurement can be used for a validation. If the strain gauge is close to a singularity in the finite element model, the stress values are very sensitive

to a small positioning error and also to geometric deviations between the casted hardware component and the virtual model derived from CAD. In this subsection, the stresses from the physical and virtual strain gauges are compared for different levels of modelling according to table 1. The evaluation of the stresses in the simulation requires a flexible modelling of the component in the MBS environment. Consequently, not all variants can be compared for all components (e.g. stresses from the knuckle can only be evaluated for a flexible model of the knuckle).

In the physical testing, a human driver rides over the tracks multiple times in a given order. This leads to slightly different excitations in every run. For the validation of the front axle model, test tracks are chosen that show only a small sensitivity with regards to velocity and lateral guidance of the bus. In figure 6, the comparison between simulated stress and measured stress from multiple runs is shown for the lower wishbone.

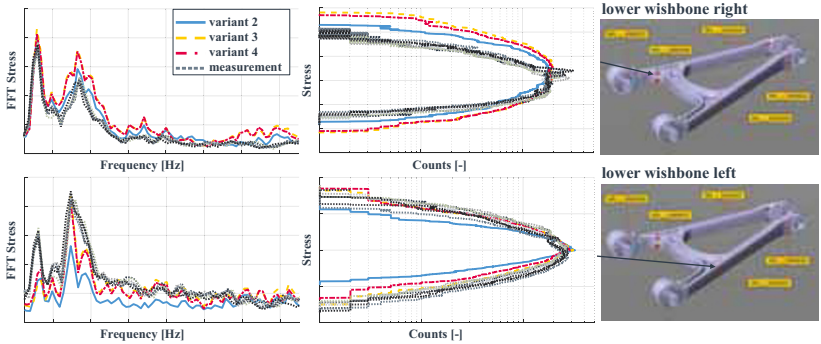

Fig. 6. Comparison of the FFT and level crossing for strain gauge 26 (top) of the right lower wishbone and strain gauge 25 (bottom) of the left lower wishbone for variant 2, 3 and 4 with measurements from various cycles.

A general improvement of both the frequency response and the load collective can be observed with increasing flexibility of the model. Especially for the strain gauge 25, it can be seen in the frequency analysis and level crossing, that the amplitude matches the measurements well if the deformation of the upper arms is taken into account.

In figure 7, a comparison of the stresses from simulation and measurement is shown for the upper arm. The frequency analysis of the stress history shows a good correlation of the peak frequencies. The peak amplitudes are underestimated in the simulation. The difference coming from a flexible modelling of the knuckle is negligible.

The comparison of the measured and simulated stress for the knuckle is depicted in figure 8. A good correlation for the peak frequencies can be observed. Looking at the stress level crossing, an offset between measurement and simulation can be seen. It results from a static pre-stress in the physical test. While the static part in the simulation can be removed with a zero load maneuver, in the real world test achieving a steady state condition without any pretension is a difficult task. Taking this into account also

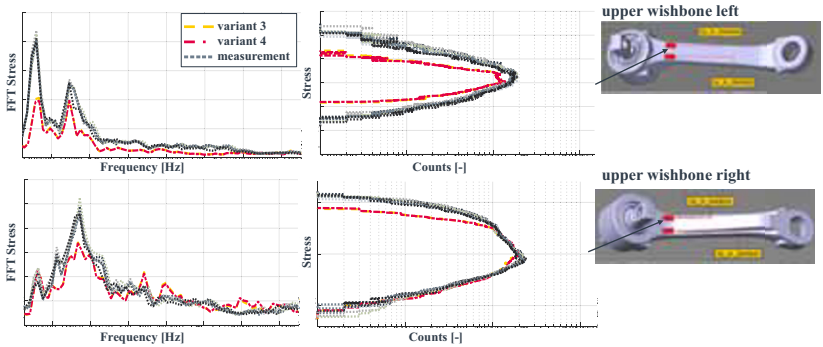

Fig. 7. Comparison of the FFT and level crossing for strain gauge 6 (top) of the left upper wishbone and strain gauge 16 (bottom) of the right upper wishbone for variant 3 and 4 with measurements from various cycles.

a good correlation for the amplitudes is given. The knuckle is a relative stiff part of the axle, which results in high Eigenfrequencies of the structure. The lowest Eigenfrequency is by far higher than the major input excitation Hence, for the description of the deformation only inertia relief modes are considered.

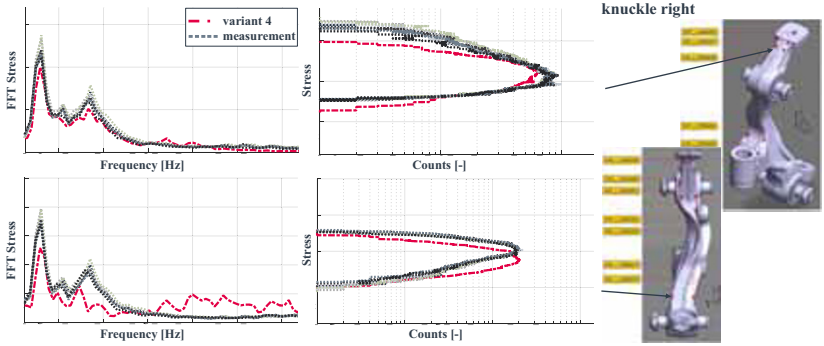

Fig. 8. Comparison of the FFT and level crossing for strain gauge 57 (top) and strain gauge 72 (bottom) of the right knuckle for variant 4 with measurements from various cycles.

5.2 Position sensitivity

The exact position of the strain gauges on the complex geometries is sometimes difficult to measure, especially when there is no landmark close to it. Furthermore, there might not exactly be a node in the finite element model at the measurement point. In this section, the sensitivity of the virtual strain gauges with respect to the position is investigated. In the multibody simulation, the virtual strain gauge elements were therefore used for the estimated position of the measurement position and the surrounding nodes. The orientation marker is kept the same. The sensitivity to the position of the strain gauge strongly depends on the stress gradient at this point. A high stress gradient,

occurring for example close to sharp edges, leads to a high sensitivity with respect to the position. The used strain gauges for the measurement are uniaxial strain gauges that only capture the stress in one direction. Consequently, it is also important to match the direction of the strain gauge. In the physical testing, the orientation of the strain gauges is aligned with the geometry, which helps to find the appropriate direction for the virtual strain gauges. In figure 9, a strain gauge with a high stress gradient in direction north-south is shown. One can observe a high dependency of the resulting stress from the evaluated node position. Other strain gauges show only a minor influence to a small shift in position.

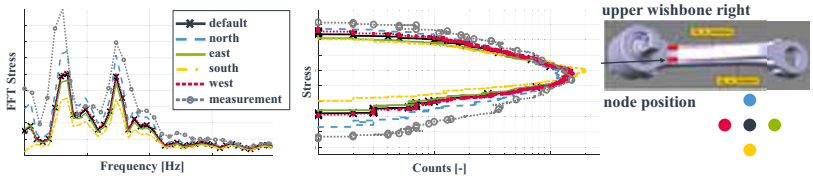

Fig. 9. Comparison of the stress FFT and level crossing for strain gauge 3 of the right upper wishbone for variant 4. The stress of the virtual strain gauge was evaluated at the nodes next to the default position.

5.3 Frame structure input loads

The comparison of the measured stress responses of the front axle parts showed a good correlation with the simulated stress responses. Only the version with the flexible bodies of the lower and upper wishbones with deformable knuckles allowed a full comparison with test data. This version also leads to the highest modelling and computational burden. Such a modelling depth is only required if the resulting forces in the bushings that connect the components to the frame show a change in comparison with the simpler front axle models.

In figure 10, the resulting bushing forces of the lower and upper wishbone for the investigated variants can be seen. For the lower arm, the force in x-direction depends mostly on the flexibility of the lower wishbone. A deformable model leads to a decrease in the force amplitude. The forces in y-direction at lower frequencies increase with added flexibility. In z-direction, the force amplitude at higher frequencies is lower if the lower arm is deformable. The straight black line in the plots shows the current cutoff frequency for the modal reduction of the frame structure. As mentioned in [12], a cutoff frequency of at least 1.5 times the excitation frequency is suggested. For the forces in z-direction this suggestion is satisfied, the forces in x- and y-direction would require a

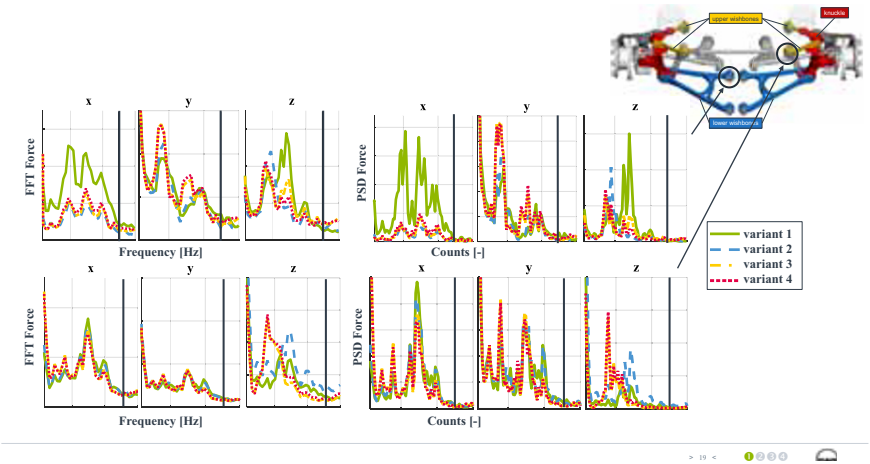

Fig. 10. Bushing forces of the left lower wishbone (top) and right upper wishbone (bottom).

slightly higher cutoff frequency, as can be seen from the fast Fourier transform and power spectral density plots. But it also has to be considered that the stress amplitude in x-direction is approximately only one tenth of the stress amplitude in z-direction.

For the upper arm, the major influence of the flexible modelling can be observed in z- direction, the influence with regard to the x- and y-directions is negligible. Looking at the cutoff frequency shown with the straight black line, one can observe that the suggestion of 1.5 times the excitation frequency holds for y- and z-direction. In x-direction, the forces are also present at slightly higher frequencies. As for the lower arm, the force amplitude in x-direction is about one dimension smaller than the amplitudes in y- and z-direction.

An accurate prediction of the transferred forces from the front axle to the frame structure requires the flexible modelling of the lower and upper wishbone. The influence of the flexibility of the knuckle on the resulting forces is negligible and consequently a rigid knuckle model can be used for an improved computation time.

6 Conclusion

The reliable prediction of the operational strength using virtual methods relies on the estimation of the input loads. While static load cases lack of accuracy for the fatigue strength determination of a vehicle structure subjected to multiaxial loading, a virtual proving ground simulation provides a more realistic prediction of the lifetime. The virtual proving ground incorporates a simulation of the vehicle response when driving over the digital twins of the real world test tracks. For an accurate lifetime simulation of the frame structure, a good prediction of the transferred loads from the road to the structure is necessary. In this work, the front axle model and loads are validated with

test data. A direct measurement of the bushing forces was not available, so the validation was performed using the strain gauge signals from axle components. Therefore, a flexible modelling of those components was required with an application of virtual strain gauges. The components used are the lower and upper wishbones and the knuckles. A good correlation between the simulated stresses and measurement values could be shown. The flexible modelling of the front axle means an increase of complexity and computation time. The necessity of the flexible modelling was investigated with a comparison of the bushing for connected to the frame structure. For an accurate prediction of the bushing forces, the deformation of the lower and upper wishbones has to be taken into account. The flexibility of the knuckle has a negligible influence on the simulated forces.

References

1. Ferry, W. B., Frise, P. R., Andrews, G. T. & Malik, M. A.: Combining virtual simulation and physical vehicle test data to optimize durability testing. In: Fatigue & Fracture of Engineering Materials & Structures, Volume 13, Issue 12, pp. 1172-1134 (2002)
2. Halfpenny, Andrew.: Methods for accelerating dynamic durability tests. In: 9th International Conference on Recent Advances in Structural Dynamics. Southampton (2006)
3. Geoportal Bayern, https://geoportal.bayern.de/bayernatlas/?lang=de&topic=ba &bgLayer=atkis&catalogNodes=11,122&E=683535.27&N=5342708.49&zoom=13&layers=luftbild, last accessed 2016/11/21.
4. Johannesson, P. & Speckert, M.: Guide to load analysis for durability in vehicle engineering, John Wiley & Sons Ltd., Chichester (2014)
5. M. Haiba, D.C. Barton, P.C. Brooks, M.C. Levesley, Review of life assessment techniques applied to dynamically loaded automotive components. Computers & Structures, Volume 80, Issues 5–6, 481-494 (2002)
6. Craig RR, Kurdila A: Fundamentals of structural dynamics, 2nd edn. John Wiley, Hoboken N.J. (2006)
7. Shabana A.A.: Modeling of Flexible Bodies. In: Pfeiffer F., Bremer H. (eds) The Art of Modeling Mechanical Systems. CISM International Centre for Mechanical Sciences (Courses and Lectures), vol 570. Springer, Cham (2017)
8. Lion A.: Application of Elastic Bodies in the Durability Simulation of Vehicles: Methods, Examples and Open Questions. In: NAFEMS Seminar: Analyse von Mehrkörpersystemen mit FEM und MKS (2004)
9. Dietz S Vibration and fatigue analysis of vehicle systems using component modes. Zugl.: Berlin, Techn. Univ., Diss. Fortschritt-Berichte VDI Reihe 12, Verkehrstechnik/Fahrzeugtechnik, vol 401. VDI-Verl., Düsseldorf (1999)
10. Herting, D.N.: A general purpose, multi-stage, component modal synthesis method, Finite Elements in Analysis and Design, Volume 1, Issue 2, pp. 153-164 (1985)
11. ANSYS Help, https://ansyshelp.ansys.com/account/secured?returnurl=/Views/Secured/corp/v191/ans_thry/thy_anproc6.html, last accessed 2020/05/04.
12. Géradin M., Cardona A.: Flexible Multibody Dynamics: A Finite Element Approach, John Wiley, Chichester (2001)